

Original Article



Trypanosoma cruzi Dysregulates piRNAs Computationally Predicted to Target IL-6 Signaling Molecules During Early Infection of Primary Human Cardiac Fibroblasts

Ayorinde Cooley ¹, Kayla J. Rayford ¹, Ashutosh Arun ¹, Fernando Villalta ^{1,2}, Maria F. Lima ², Siddharth Pratap ³, Pius N. Nde ^{1,*}

¹Department of Microbiology, Immunology and Physiology, Meharry Medical College, Nashville, TN 37208, USA

²Department of Cell, Molecular, and Biomedical Sciences, School of Medicine, The City College of New York, New York, NY 10031, USA

³School of Graduate Studies and Research, Meharry Medical College, Nashville, TN 37208, USA

OPEN ACCESS

Received: Mar 17, 2022

Revised: Sep 20, 2022

Accepted: Oct 26, 2022

Published online: Dec 2, 2022

*Correspondence to

Pius N. Nde

Department of Microbiology, Immunology and Physiology, Meharry Medical College, 1005 Dr DB Todd Jr Blvd, Nashville, TN 37208, USA.
Email: pnnde@mmc.edu

Copyright © 2022. The Korean Association of Immunologists

This is an Open Access article distributed under the terms of the Creative Commons Attribution Non-Commercial License (<https://creativecommons.org/licenses/by-nc/4.0/>) which permits unrestricted non-commercial use, distribution, and reproduction in any medium, provided the original work is properly cited.

ORCID iDs

Ayorinde Cooley

<https://orcid.org/0000-0002-8710-6910>

Kayla J. Rayford

<https://orcid.org/0000-0002-9493-3439>

Ashutosh Arun

<https://orcid.org/0000-0003-0161-0727>

Fernando Villalta

<https://orcid.org/0000-0002-6232-0574>


Maria F. Lima

<https://orcid.org/0000-0001-8835-5700>

ABSTRACT

Trypanosoma cruzi, the etiological agent of Chagas disease, is an intracellular protozoan parasite, which is now present in most industrialized countries. About 40% of *T. cruzi* infected individuals will develop severe, incurable cardiovascular, gastrointestinal, or neurological disorders. The molecular mechanisms by which *T. cruzi* induces cardiopathogenesis remain to be determined. Previous studies showed that increased IL-6 expression in *T. cruzi* patients was associated with disease severity. IL-6 signaling was suggested to induce pro-inflammatory and pro-fibrotic responses, however, the role of this pathway during early infection remains to be elucidated. We reported that *T. cruzi* can dysregulate the expression of host PIWI-interacting RNAs (piRNAs) during early infection. Here, we aim to evaluate the dysregulation of IL-6 signaling and the piRNAs computationally predicted to target IL-6 molecules during early *T. cruzi* infection of primary human cardiac fibroblasts (PHCF). Using in silico analysis, we predict that piR_004506, piR_001356, and piR_017716 target *IL6* and *SOCS3* genes, respectively. We validated the piRNAs and target gene expression in *T. cruzi* challenged PHCF. Secreted IL-6, soluble gp-130, and sIL-6R in condition media were measured using a cytokine array and western blot analysis was used to measure pathway activation. We created a network of piRNAs, target genes, and genes within one degree of biological interaction. Our analysis revealed an inverse relationship between piRNA expression and the target transcripts during early infection, denoting the IL-6 pathway targeting piRNAs can be developed as potential therapeutics to mitigate *T. cruzi* cardiomyopathies.

Keywords: *Trypanosoma cruzi*; Interleukin-6; RNA, small untranslated; Parasites; Immunity; RNA, small interfering

Siddharth Pratap 
<https://orcid.org/0000-0003-2200-0848>

 Pius N. Nde 
<https://orcid.org/0000-0001-7101-7721>

Conflict of Interest

The authors declare no potential conflicts of interest.

Abbreviations

Ct, cycle threshold; ECM, extracellular matrix; EGF, epidermal growth factor; IL-6R, IL-6 receptor; mbgp-130, membrane-bound gp-130; miRNA, micro RNA; MITF, melanocyte inducing transcription factor; mRNA, messenger RNA; PFA, paraformaldehyde; PHCF, primary human cardiac fibroblasts; PHCM, primary human cardiac myocytes; piRNA, PIWI-interacting RNA; PRKCD, protein kinase C delta; p-STAT3, phosphorylated STAT3; PTK2B, protein tyrosine kinase 2 beta; qPCR, quantitative real-time PCR; RHM, rat heart myoblast; RPLPO, ribosomal protein, lateral stalk subunit P0; sgp-130, soluble gp-130; sIL-6R, soluble IL-6 receptor; snRNA, small non-coding RNA; SOCS3, suppressor of cytokine signaling 3; UTR, untranslated region.

Author Contributions

Conceptualization: Nde PN; Formal analysis: Cooley A, Rayford KJ, Nde PN; Funding acquisition: Rayford KJ, Villalta F, Lima MF, Nde PN; Investigation: Nde PN; Methodology: Cooley A, Rayford KJ, Arun A, Villalta F, Lima MF, Pratap S, Nde PN; Project administration: Nde PN; Resources: Villalta F, Lima MF, Pratap S, Nde PN; Supervision: Villalta F, Pratap S, Nde PN; Validation: Cooley A, Rayford KJ, Arun A, Pratap S, Nde PN; Visualization: Cooley A, Rayford KJ, Arun A, Pratap S, Nde PN; Writing - original draft: Cooley A, Rayford KJ, Nde PN; Writing - review & editing: Cooley A, Rayford KJ, Arun A, Villalta F, Lima MF, Pratap S, Nde PN.

INTRODUCTION

Trypanosoma cruzi, the etiological agent of Chagas disease, is an intracellular protozoan parasite, which affects several million individuals causing severe economic burden (1,2). Though originally endemic to Central and South America, it is now present in all industrialized regions of the globe due to modern globalization. Approximately 40% of those infected with *T. cruzi* will develop cardiovascular, gastrointestinal, or neurological disorders (3,4). Current therapeutics only treat the acute phase of infection with severe side effects. Thus, there is a need to understand the molecular mechanisms of *T. cruzi* pathogenesis to facilitate identification of biomarkers and new therapeutic targets. The IL-6 signaling pathway has been suggested to play important roles in experimental and clinical *T. cruzi* pathogenesis (5-7). IL-6 is a cytokine with diverse roles in endothelial cell function, inflammation, and fibrogenesis (8-11). IL-6 signaling is critical in driving local inflammation and activating immune responses in endothelial cells and fibroblasts (12,13). The cytokine is transiently expressed in response to biological stimuli or environmental stress such as tissue injury or infection to activate host defense against the stressor, prompting an acute inflammatory response (14). During inflammation, IL-6 signaling induces transition to a reparative environment at the injury site (15,16), which is followed by deposition of extracellular matrix (ECM) proteins including type I collagen (17). IL-6 stimulates the migration of fibroblasts to sites of injury and drives myofibroblast activation (18). Myofibroblasts are the primary producers of ECM proteins, inflammatory and fibrogenic cytokines (19,20).

In humans, the IL-6 receptor (IL-6R) is only expressed in hepatocytes, myeloid, and lymphoid lineage cells (21). Other cell types that do not express IL-6R, respond to IL-6 primarily through trans-signaling (22) where soluble IL-6 binds to soluble IL-6R (sIL-6R), produced from cleavage or secretion of IL-6R from neutrophils (23) and other cells. The IL-6/sIL-6R complex formed can then bind to the ubiquitously expressed membrane-bound gp-130 (mbgp-130) receptor on target cells (15) to activate STAT3 through JAK-STAT protein phosphorylation (15). Phosphorylated STAT3 (p-STAT3) dimerizes and translocate to the nucleus to function as a transcription factor for IL-6 response genes (24). IL-6 signaling acts synergistically with the TGF- β /Smad3 signaling pathway to promote the production of p-STAT3 (16,25). Furthermore, it has been suggested that IL-6 promotes the activation of TGF- β via STAT3 activation (25). Suppressor of cytokine signaling 3 (SOCS3) negatively regulates IL-6 signaling by binding to gp-130 and inhibiting JAK kinase activity, thereby preventing STAT3 phosphorylation (24). Soluble gp-130 (sgp-130) binds to the IL-6/sIL-6R complex and competitively prevents it from binding to the mbgp-130 receptor to downregulate IL-6 signaling (26). IL-6 is a pleiotropic cytokine that can function as a proinflammatory or profibrotic factor depending on the cellular context (27). IL-6 increases the activation of cardiac fibroblasts. Activated cardiac fibroblasts can produce significantly increased IL-6 in combination with other cells including macrophages and cardiomyocytes compared to cardiac fibroblasts alone (28,29). Dysfunctional IL-6 signaling has been associated with different forms of cardiomyopathy, including cardiac hypertrophy, arrhythmias, and myocardial fibrosis (9,30,31).

High levels of IL-6 has been associated with disease severity in Chagas disease patients and murine model of *T. cruzi* infection (32,33). A recent study suggested that inhibition of STAT3 led to worsening of cardiac function in a murine model of *T. cruzi* infection through unknown mechanisms (6). We and others showed that *T. cruzi* upregulates the transcript and protein

levels of IL-6 during early infection of cardiomyocytes and inflammatory cells (34-36). However, IL-6 expression and signaling during *T. cruzi* infection in other cardiac cell types, including fibroblasts and endothelial cells, remain unknown. Characterizing the host early molecular responses to *T. cruzi* infection is vital in understanding the pathogenesis of *T. cruzi* infection and identifying potential biomarkers and therapeutic targets.

PIWI-interacting RNAs (piRNAs) are a class of small non-coding RNA (sncRNA) that have recently been shown to regulate genome rearrangement, epigenetic regulation, transcription, and translation (37). These piRNAs are the most abundant class of sncRNA and are emerging as regulators of critical biological processes, making it essential to elucidate their roles in disease pathogenesis (37,38). Numerous piRNAs were first identified through sequencing of small RNA from human testes (39). While their genomic coordinates and presence within piRNA clusters were confirmed, no further characterization of these piRNAs were conducted (39). Despite the abundance of piRNAs, their exact regulatory mechanisms remain undeciphered (37). Others suggested that piRNAs regulate the expression of interleukins in CD4⁺ T-Cells (40). Our group showed that piRNAs are dysregulated by *T. cruzi* during early infection in primary human cardiac myocytes, albeit their specific roles remain undefined (41).

Using RNA-Seq, we identified piRNAs piR_004506 (DQ576200), piR_001356 (DQ571873), and piR_017716 (DQ594453) from Girard et al. (39) to be expressed in *T. cruzi* challenged primary human cardiac myocytes (PHCM) (41). Though these piRNAs were not differentially expressed in PHCM, we proceeded to evaluate their expression in parasite challenged primary human cardiac fibroblasts (PHCF), as piRNA expression can be cell type dependent (42,43). We observed that the parasite dysregulated the expression of host-derived piRNAs piR_004506, piR_001356, and piR_017716 computationally predicted to target *IL6* and *SOCS3*, respectively. We found an inverse relationship between piRNA expression and the expression of their target gene transcripts. We also observed a gradual decrease in IL-6 in condition media, a significant increase of p-STAT3 at 6 h post-challenge, and a continual significant decrease of SOCS3. We used these biomolecules to create a network of interconnected genes illustrating IL-6 pathway protein-protein interactions and the dysregulated piRNA expressions during early *T. cruzi* infection in PHCF. Taken together, this report illustrates the interplay between piRNAs targeting IL-6 signaling pathway molecules during the early phase of *T. cruzi* infection.

MATERIALS AND METHODS

Primary human cardiac fibroblasts culture

PHCF low passage, was grown according to the manufacturer's recommendations (PromoCell, Heidelberg, Germany). Briefly, PHCFs were cultured in fibroblast basal growth medium supplemented with the supplemental mix (PromoCell) containing fetal calf serum (0.1 ml/ml), recombinant human epidermal growth factor (0.5 ng/ml), recombinant human basic fibroblast growth factor (2 ng/ml) and recombinant human insulin (5 ug/ml). The cells were grown in T75 flasks at 37°C in the presence of 5% CO₂ to a confluence of about 80% (about 4×10⁶ cells) before being used in the *T. cruzi* infection and control assays.

Parasite culture and infection assays

Rat heart myoblast (RHM) monolayers at 80% confluence, cultured in complete DMEM containing glutamax, 20% FBS, 1% each of penicillin/streptomycin, multivitamins, and MEM

non-essential amino acids (Life Technologies, Carlsbad, CA, USA) were infected with *T. cruzi* trypomastigotes. Pure cultures of highly invasive *T. cruzi* trypomastigotes clone MMC 20A (Tulahuen strain) were harvested from the supernatant of RHM monolayers as previously described (44). The parasites were washed in HBSS and resuspended in PHCF growth medium without supplement at 1×10^7 parasites/ml. For the infection assays, PHCF confluent monolayers were starved in HBSS containing 30 mM HEPES followed by the addition of invasive *T. cruzi* trypomastigotes in fibroblast basal growth medium without supplements at a ratio of 10 parasites per cell. The cells challenged with the parasites were incubated for different time points: 1, 3, and 6 h. Each time point was prepared using three independent T75 flasks to extract total and small RNA and three independent T75 flasks for use in the western blotting experiment.

RNA extraction

At each designated time point of the experiment, the parasites were washed off the PHCF cells, and the cells were lysed in Qiazol (Qiagen, Valencia, CA, USA) as described by the manufacturer. Total and small RNA molecules were purified with the miRNeasy Mini purification kit (Qiagen). The RNA purification step included an on-column DNase treatment step to eliminate traces of genomic DNA as described by the manufacturer (Qiagen). The quality of the purified RNA was analyzed using the Bioanalyzer 2100 system (Agilent Technologies, Santa Clara, CA, USA). High-quality purified RNA with RNA integrity number of at least eight were used for further analysis.

Quantitative real-time PCR

Quantitative real-time PCR (qPCR) was done to validate the microarray data using a customized PrimePCR assay (Bio-Rad, Hercules, CA, USA) containing the genes of interest. In the PrimePCR array experiment, total RNA (1 μ g) was converted to cDNA using the iScript cDNA synthesis kit, essentially as described by the manufacturer (Bio-Rad). The generated cDNA was mixed with SsoAdvanced SYBR green 2X master mix and loaded (20 μ l/per well) on a customized PrimePCR plate containing primers for selected genes to be validated, including housekeeping genes and controls as described (www.bio-rad.com/PrimePCR). The PCR amplification was carried out on a C1000 Touch Thermal Cycler as described by the manufacturer (Bio-Rad). The cycle threshold (Ct) values of housekeeping genes (beta-2 microglobulin, ribosomal protein lateral stalk subunit P0 [RPLP0] and, beta-actin) were checked for consistency on all plates across all samples. The data were normalized against the housekeeping genes and control samples using CFX manager analysis software with support from Bio-Rad technical service using the $\Delta\Delta$ Ct method. The primer sequences used for quantification of the transcript levels in the PrimePCR were not disclosed by Bio-Rad.

For piRNA quantification, we used the TaqMan Small RNA Assay essentially as described by the manufacturer (Thermo Fisher Scientific, Waltham, MA, USA). Briefly, piRNA-specific stem-loop RT primers were used to create each cDNA template. For each piRNA, a TaqMan primer-probe set was utilized to amplify each target cDNA by TaqMan qPCR, using U6 as a housekeeping sncRNA. TaqMan real-time PCR assays were carried out on a CFX96 Thermal Cycler (Bio-Rad) as per Thermo Fisher Scientific recommendations. The Ct values of housekeeping gene U6 were checked for consistency on all plates across all samples. The data were normalized against the housekeeping U6 and control samples using CFX manager analysis software using the $\Delta\Delta$ Ct method. The primer sequences used to quantify the piRNA levels in the TaqMan Small RNA were not disclosed by Thermo Fisher Scientific.

Immunoblotting

Western blot assays were performed as previously described (44). Briefly, serum-starved PHCF cells (about 80% confluence on a T75 flask) challenged with *T. cruzi* trypomastigotes or media alone were lysed in NP40 Cell Lysis Buffer (Life Technologies) in the presence of phosphatase inhibitor cocktails 2 and 3 at 1:100 each, (Sigma Aldrich, St. Louis, MO, USA) and protease inhibitor cocktail set III at 1:100, (Calbiochem, Gibbstown, NJ, USA). Whole cell lysates (20 µg/lane) were separated by SDS-PAGE on a 4%–15% gradient polyacrylamide gel and transferred onto nitrocellulose membranes (Life Technologies). The membranes were incubated for 1 h in TBS Intercept blocking buffer (LI-COR Biosciences, Lincoln, NE, USA) followed by incubation with the following Abs: mouse anti-STAT3 Ab (1:1,000), rabbit anti-p-STAT3 Y705 Ab (1:1,000), rabbit anti-SOCS3 (1:1,000), and mouse anti-GAPDH Ab (1:10,000), in blocking buffer at 4°C overnight. The blots were washed and incubated with the corresponding secondary Abs IRDye 680 donkey anti-mouse 1:20,000 and IRDye 800 donkey anti-rabbit (LI-COR Biosciences) in blocking buffer for 1 h at room temperature. The blots were washed and scanned using the infrared fluorescence detection Odyssey Imaging Systems (LI-COR Biosciences) to visualize the bound Ab. Housekeeping GAPDH signal was used for the normalization of loading differences. Each experimental biological replicate was done in triplicate. Protein bands were analyzed and quantified with ImageJ (45) (<https://imagej.nih.gov/ij>). The detected band intensities for each *T. cruzi*-treated sample group were compared to the non-treated control group using a Student's *t*-test or one-way ANOVA (non-parametric; $p \leq 0.05$) with a *post hoc* Newman–Keuls test. The normalized ratio of protein expression level was defined as the ratio of the target protein band intensity to the internal control protein density (GAPDH) of 1.0. These data were collected from three independent experiments.

Human cytokine Ab array

To analyze the cytokine expression in condition media of *T. cruzi*-infected primary cardiac fibroblasts, we used a commercially available Human Cytokine Array C100 following the manufacturer's protocol (RayBiotech, Peachtree Corners, GA, USA). This is a membrane-based sandwich immunoassay kit where the capture Abs against cytokines, chemokines, and other secreted molecules, and control proteins are spotted in duplicates on nitrocellulose membranes to bind specific target proteins present in the condition media. Briefly, blocked array membranes were incubated with condition media from *T. cruzi* infected cells at various time points (0, 1, 3, and 6 h) at 4°C overnight on a platform shaker. Washed membranes were further incubated with biotinylated Ab cocktails for two hours at room temperature on a rocking platform. The membranes were washed, probed with streptavidin-HRP, and visualized by chemiluminescence using ChemiDoc Imager (Bio-Rad). The blots were scanned, and the density of each spot was quantified against the average of the internal controls as recommended by the manufacturers (RayBiotech). Densitometric analysis were completed using ImageJ.

Cell surface staining for IL-6R and gp130

PHCF monolayers challenged with *T. cruzi* were washed 2X with Dulbecco's phosphate-buffered saline, trypsinized using TripleE (Thermo Fisher Scientific), neutralized with TNS (PromoCell) and spun down at 1,300 rpm for 3 min. Cells were resuspended in 5 ml of 1% FACS buffer (5 mL FBS in 500 mL PBS) and counted. About 1×10^6 cells were used for staining for each time point. Cells were stained with anti-CD130-Biotin (Cat. No. 46-4714-82) for 30 min at 4°C, followed by Streptavidin-PE (12-4317-87), anti-CD126-PerCP-eFluor 710 (Cat. No. 46-1269-42), and LIVE/DEAD Fixable Aqua Dead Cell Stain (Cat. No. 17-4321-81) for another 30 min at 4°C. Cells were stained following the manufacturer's recommendations. The stained cells were washed 2X

with FACS buffer, fixed with 4% paraformaldehyde (PFA) for 5 min and resuspended in PBS. Data was acquired and analyzed on Amnis CellStream Flow Cytometer. Data was analyzed and visualized using GraphPad Prism software (GraphPad Software, Inc., La Jolla, CA, USA). All Abs and isotypes controls were from Thermo Fisher Scientific.

Biological interaction network

Biological interaction network construction was conducted with GeneMANIA (Gene Function Prediction using a Multiple Association Network Integration Algorithm; <https://genemania.org>) (46). This tool constructs networks using publicly available datasets containing data on gene expression, genetic interactions, protein domains, subcellular localization, biochemical reactions, pathways, and protein interactions. Of the available data sources, we filtered our network to contain interactions from Pathway data (searches Reactome and BioCyc) and physical/protein-protein interaction data (searches BioGrid, PathwayCommons, among others). We queried *IL6*, *IL6R*, *gp130 (IL6ST)*, *STAT3*, and *SOCS3* using Homo sapiens as the reference organism and combined the results with our piRNA target prediction data. The combined network was visualized with Gephi ver. 0.9.2 (<https://gephi.org>)

Statistical analysis

A 2-tailed Student's *t*-test was performed for single comparisons of 2 groups. A one-way ANOVA with a *post hoc* Newman-Keuls test was performed to determine significant differences among multiple groups. In all analyses, $p \leq 0.05$ was considered statistically significant. All statistical analyses were performed using GraphPad Prism (GraphPad Software, Inc.).

RESULTS

In silico analysis predicts piRNAs targeting *IL6* and *SOCS3* early during *T. cruzi* infection of PHCF

We used miRanda to predict interactions between target messenger RNA (mRNA) and piRNAs. Our analysis showed that piR_004506 targeted an exonic region of *IL6* mRNA transcript (Fig. 1A). The 3' untranslated region (UTR) of *SOCS3* was targeted by piR_001356 and piR_017716 (Fig. 1B). Other studies suggested that disruption of IL-6 expression and downstream targets during parasite infection play important roles in *T. cruzi* pathogenesis (5-7,47). These results suggest that these piRNAs may be important modulators of *IL6* and *SOCS3* gene expression during the early/acute phase of *T. cruzi* infection and pathogenesis.

Trypanosoma cruzi dysregulates *IL6*, *SOCS3*, and target piRNAs expressions during early infection in PHCF

Since the IL-6 pathway has been shown to be important in *T. cruzi* pathogenesis (6,47), we decided to evaluate the expression of those piRNAs in *T. cruzi* challenged PHCF because their differential expression could be context dependent (41-43). To evaluate the expression of *IL6*, *SOCS3*, and the piRNAs of interest that can target them, we challenged PHCF with *T. cruzi* trypomastigotes for various time points (0, 1, 3, and 6 h), and extracted total and small RNAs for our RT-qPCR assays. We found that the relative expression of *IL6* transcript displayed a significant decrease during our experimental window of early infection (Fig. 2A). Similarly, *SOCS3* transcript exhibited decreased relative expression at 1 and 3 h followed by an insignificant increase at 6 hrs relative to the 0 h control (Fig. 2B). We evaluated the relative expression of piRNAs piR_004506, piR_001356, and piR_017716, predicted to target *IL6* and *SOCS3*. We found that piR_004506, predicted to target *IL6*, exhibited a significant

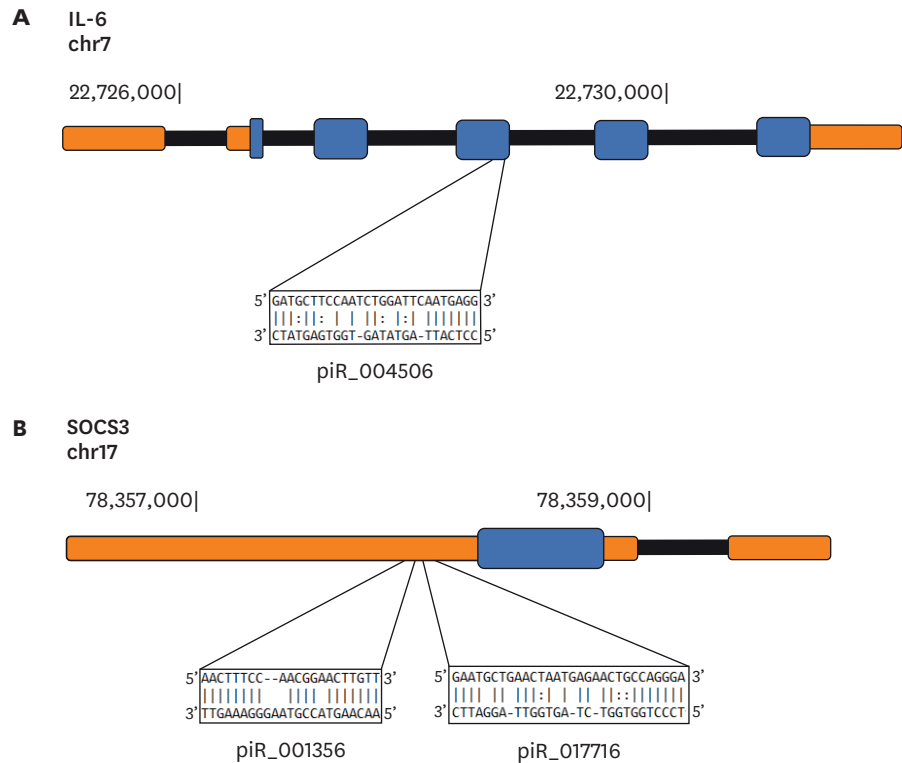


Figure 1. Mapping differentially expressed piRNAs to specific genetic regions of *IL6* and *SOCS3*. The targets of differentially expressed piRNAs in PHCF challenged with *T. cruzi* were computationally predicted using the miRanda algorithm. In the genetic cartoons, exons represented by blocks (blue) are connected by horizontal lines representing introns, while the 5' and 3' UTRs are represented as thinner blocks (orange) at the extremities of each gene, respectively. (A) *IL6* gene cartoon (5' to 3' orientation) showing the position where the differentially expressed piR_004506 is predicted to map. (B) Cartoon of *SOCS3* gene (3' to 5' orientation) showing positions where known piRNAs piR_001356 and piR_017716 map to the 3' UTR region of *SOCS3*.

relative increase at 1 h followed by an insignificant relative decrease at 3 and 6 h after parasite challenge, which remained higher than the control (**Fig. 2C**). *SOCS3* targeting piRNAs, piR_001356 and piR_017716 showed significant increased expression relative to control. The expression of piR_001356 was significantly higher at 1 and 3 h followed by a significant decrease at 6 h compared to control (**Fig. 2D**). Relative expression of piR_017716 showed a non-significant increase at 1 and 3 h and a significant decrease at 6 h following parasite challenge compared to control (**Fig. 2E**). These results show an inverse relationship between target mRNA and their corresponding piRNA expressions suggesting that these specific piRNAs potentially negatively regulate *IL6* and *SOCS3*. The results also suggest that piRNA expression can vary in different cell types following parasite challenge.

Parasite challenged PHCF exhibited alterations in IL-6 signaling molecules in condition media during early infection

We and others showed that IL-6 is differentially expressed during *T. cruzi* infection in different contexts; however, the expression during early infection of PHCF remains undefined. To gain insight into parasite-induced alterations in cytokine secretion during acute infection of PHCF, we utilized a human cytokine array. We challenged PHCF with *T. cruzi* for different time points and analyzed cytokine secretion in condition media following parasite challenge. With a particular interest in IL-6 signaling proteins, we evaluated the expression of IL-6, sIL-6R, and sgp-130 expression. The C6 and C7 arrays were incubated with condition media overnight

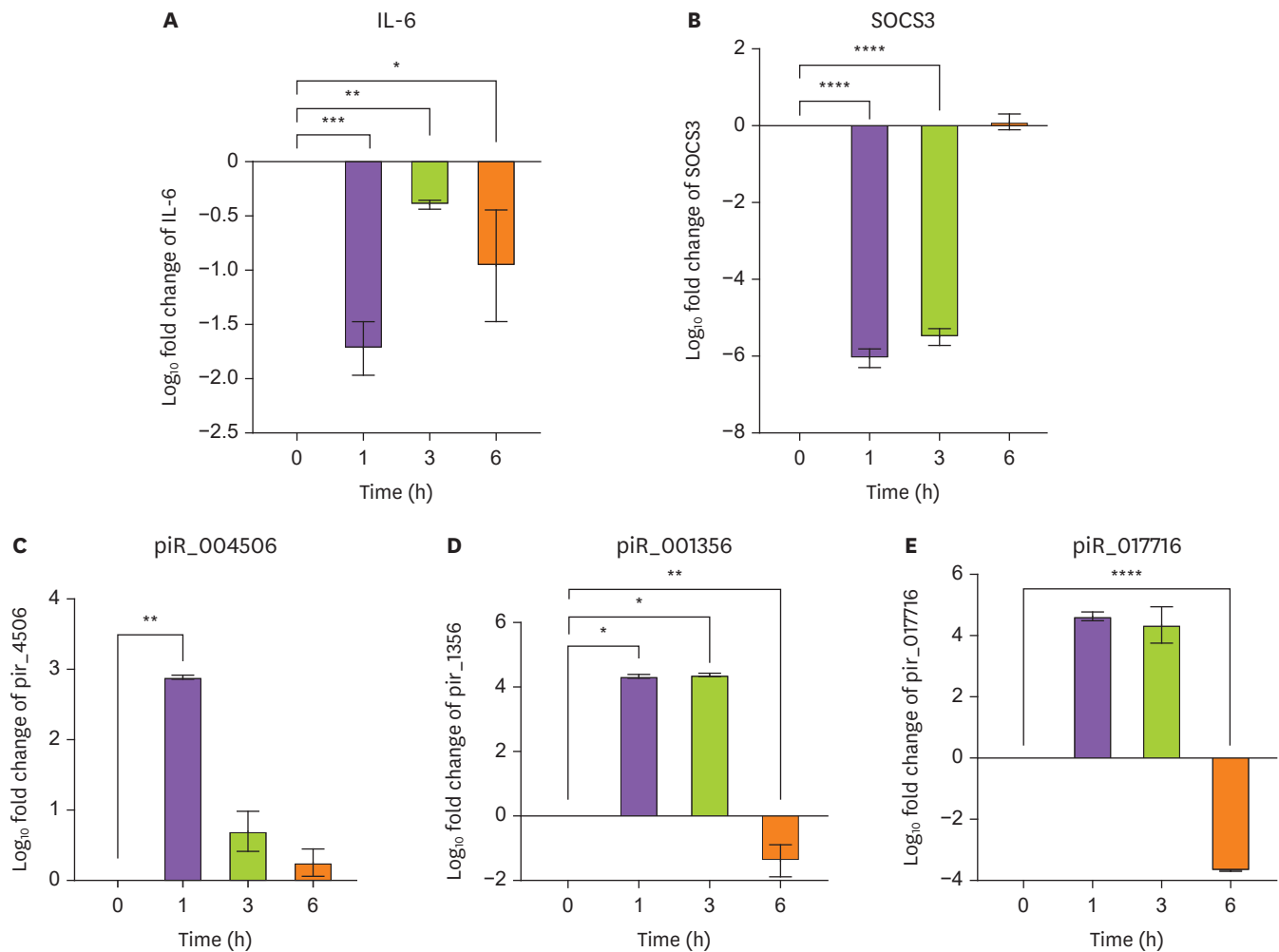


Figure 2. Validation of piRNAs and target transcript expression during early *T. cruzi* infection in PHCF. Small and total RNAs purified from serum-starved PHCF monolayers challenged with invasive *T. cruzi* trypomastigotes for different time points were used to validate (A) *IL6*, (B) *SOCS3* transcripts, (C) piR_004506, (D) piR_001356, and (E) piR_017716. Relative expression of each transcript was normalized against ribosomal protein lateral stalk subunit P0 and beta-2-microglobulin as housekeeping genes. Relative expression of each piRNA was normalized against U6. Each value is the mean of biological triplicates performed in technical duplicates \pm SEM. Visualization was created, and statistical significance was calculated using Student's *t*-test in GraphPad Prism. * $p < 0.05$, ** $p < 0.01$, *** $p < 0.001$, **** $p < 0.0001$.

and developed by chemiluminescence (Fig. 3A). Accordingly, we found that the level of IL-6 in the condition media of parasite challenged PHCF showed an insignificant gradual decrease at 1 and 3 h, with a significant decrease occurring at 6 h after parasite challenge (Fig. 3B). In contrast, sIL-6R showed a significant increase at 1 h followed by an insignificant increase at 3 and 6 h after parasite challenge compared to control (Fig. 3C). Interestingly, the levels of sgp-130 showed a pattern similar to that of sIL-6R; increased expression in condition media reached maximum levels at 1 hour after parasite challenge followed by an insignificant increase at 3 and 6 h following parasite challenge compared to control (Fig. 3D). We also evaluated the expression of membrane bound IL-6R and gp-130 and found no significant changes in expression during parasite challenge (Supplementary Fig. 1). These data suggest that other cells are required to work in collaboration with PHCF to produce high IL-6 during *T. cruzi* infection.

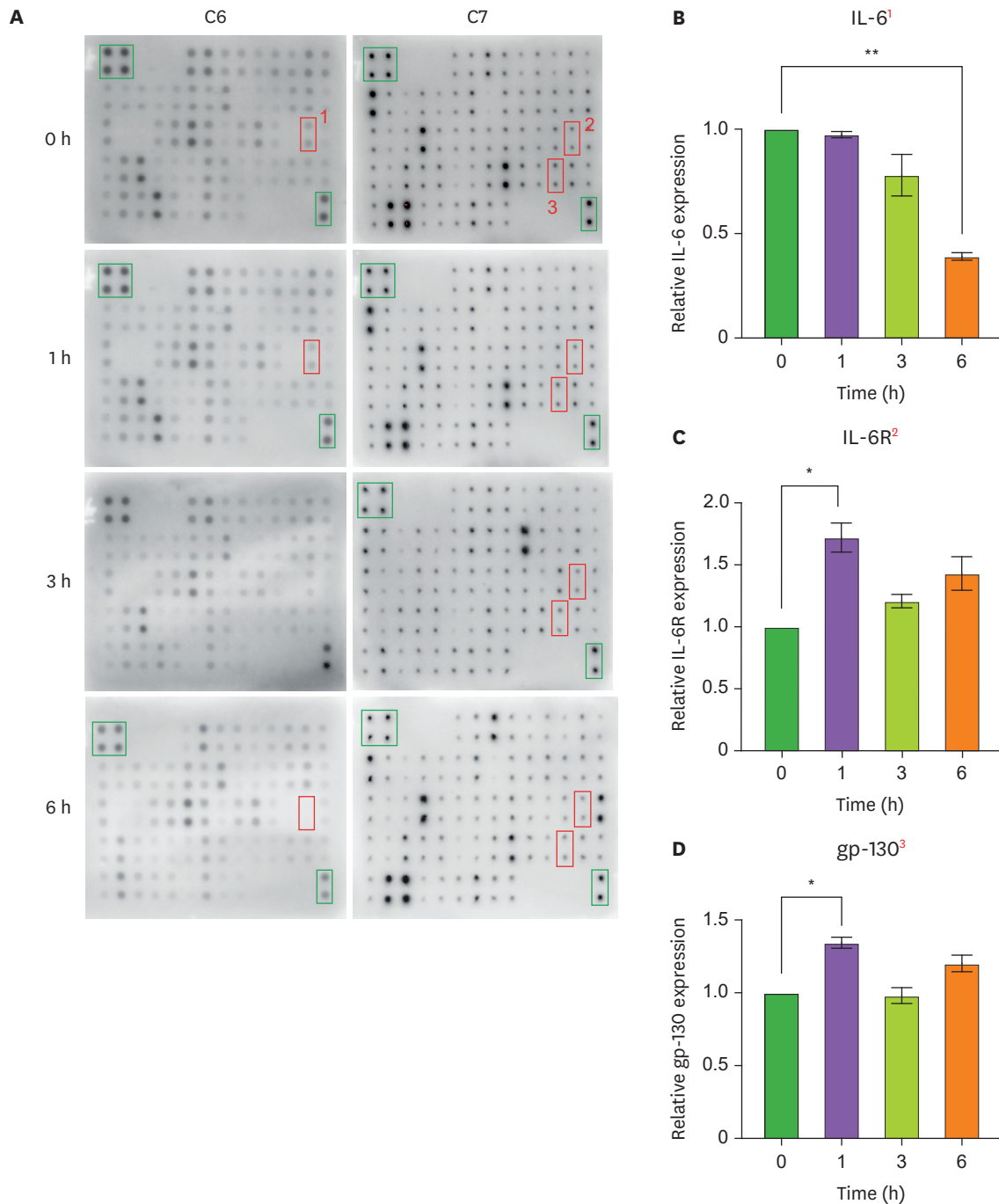


Figure 3. Cytokine array analysis evaluating IL-6 signaling proteins in condition media of *T. cruzi* challenged PHCF. Condition media of PHCF challenged with *T. cruzi* at multiple time points were incubated with cytokine array membranes C6 and C7. (A) Membranes showing the location of controls (green borders) cytokines and inflammatory molecules spotted onto a human cytokine array membranes. Signals of IL-6, IL-6R, and gp-130 at 0, 1, 3, and 6 h are indicated by numbers 1-3, respectively. Spots were quantified using ImageJ and normalized to positive control spots (green borders). Bar graphs depict fold change of (B) IL-6, (C) IL-6R, and (D) gp-130 mean spot densities relative to positive controls in condition media of PHCF *T. cruzi* challenged cells. Mean values of biological replicates \pm SEM are shown. Visualization was created, and statistical significance was calculated using Student's *t*-test in GraphPad Prism. * $p < 0.05$, ** $p < 0.01$.

Trypanosoma cruzi infection alters activation and expression of downstream IL-6 signaling proteins p-STAT3 and SOCS3, respectively

Accumulating evidence implicates activation of STAT3 via IL-6 signaling as a potential profibrotic transcription factor. Hoffman et al. (6) showed that STAT3 inhibition attenuated the expression of profibrotic molecules and the induction of cardiac fibrosis in a Chagasic Cardiomyopathy murine model. To assess the activation of canonical IL-6 signaling, we evaluated the phosphorylation of STAT3 and protein expression of SOCS3 in PHCF challenged cells compared to controls. We found that the levels of p-STAT3 Y705 in cell lysates remained steady and showed a significant increase at 6 hrs (1.1581±0.02647) following parasite challenge in PHCF compared to control (Fig. 4A). In contrast, SOCS3 showed a continuous significant decrease at 1 h (0.87138±0.01), 3 h (0.762356±0.08) and 6 h (0.747389±0.07) following parasite challenge compared to control (Fig. 4B). We evaluated the expression levels of other cytokines known to activate p-STAT3, which did not show consistent significant increase during the course of parasite challenge (Supplementary Fig. 2). These results show that the activation and protein expression of downstream IL-6 signaling molecules p-STAT3 and SOCS3, respectively, are dysregulated during early infection of PHCF by *T. cruzi*.

Biological interaction network of differentially expressed piRNA and IL-6 signaling pathway

We generated a biological interaction network to evaluate connectivity of genes involved in the IL-6 signaling axis in PHCF during early phase of *T. cruzi* infection. The GeneMANIA (http://genemania.org) program was used to identify genes related to *IL6*, *IL6R*, *gp-130*, *IL6ST*, *STAT3*, and *SOCS3*, expanding this set of genes out to one degree of molecular protein-protein and pathway level interactions. The resulting interaction network of 24 genes was combined with the predicted piRNA-target interactions (Fig. 5). The genes in the network

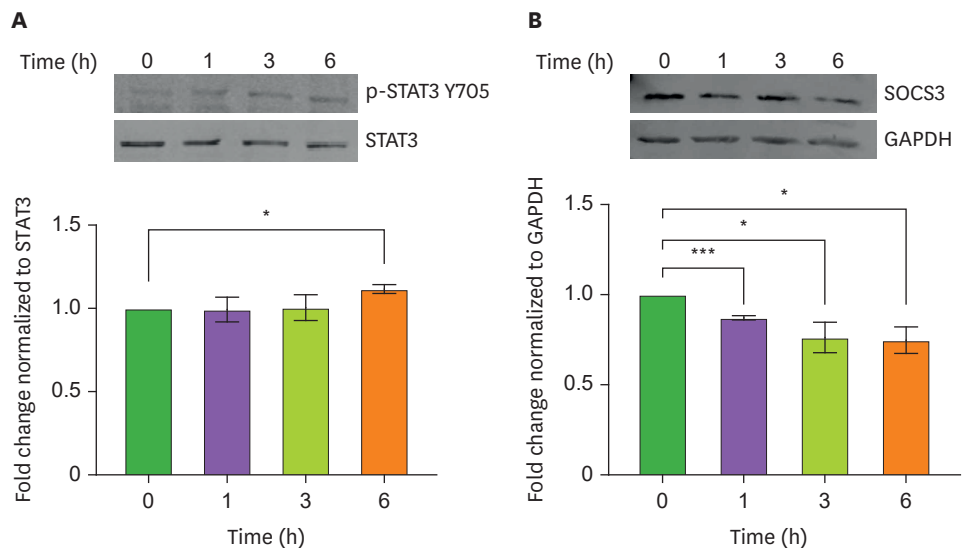


Figure 4. Expression of downstream IL-6 signaling proteins during early *T. cruzi* infection of PHCF. Whole cell lysates from PHCF challenged with *T. cruzi* at various time points were resolved by SDS-PAGE, transferred to nitrocellulose membranes, and probed with Abs against (A, upper panel) p-STAT3, and STAT3, (B, upper panel) SOCS3, and GAPDH and developed with the corresponding IRDye conjugated secondary Ab. The developed blots were scanned using the infrared fluorescence detection Odyssey Imaging System. The normalized fold changes were determined and plotted in the bar graph (A, lower panel) p-STAT3 Y705 and (B, lower panel) SOCS3. Graph bars represent mean values ± SEM from three independent biological replicates. Visualization was created, and statistical significance was calculated using Student’s t-test in GraphPad Prism. *p<0.05, ***p<0.001.

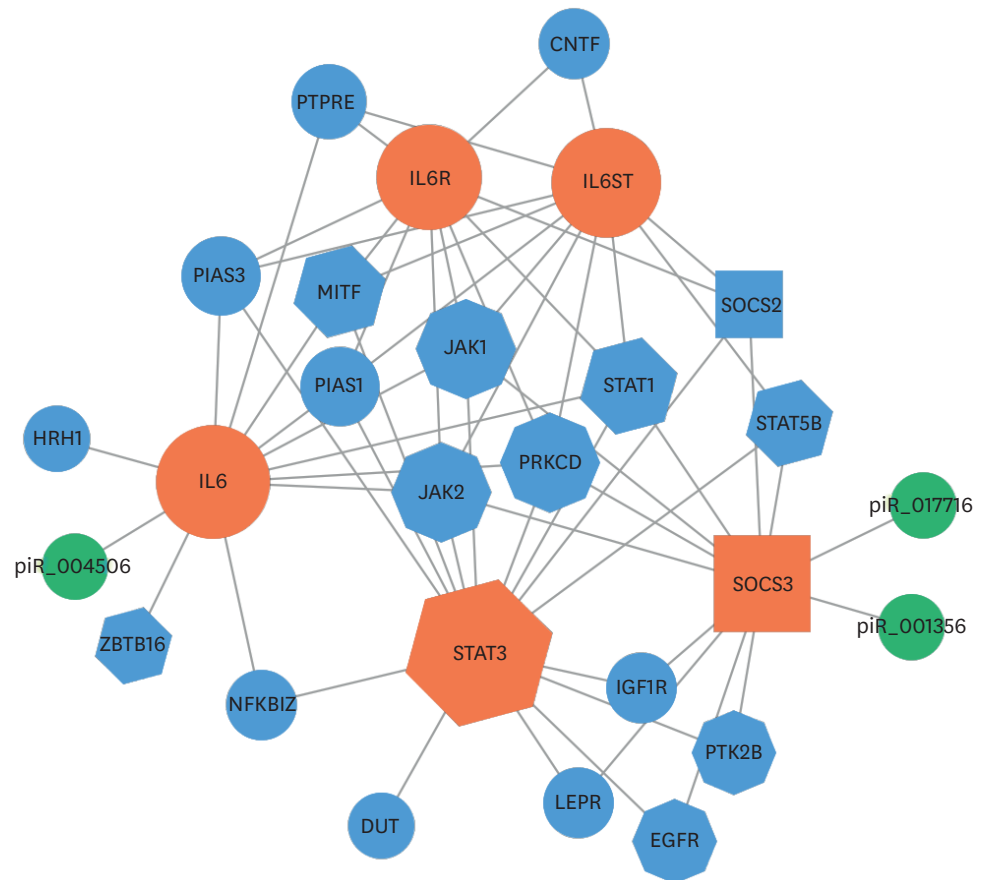


Figure 5. Biological interaction network of IL-6 signaling proteins. Network constructed based on genes from GeneMANIA using *IL6*, *IL6R*, *gp130/IL6ST*, *STAT3*, and *SOCS3* as the query input. The gray connections represent protein-protein and pathway-level interactions between the query proteins and the expanded gene set. Predicted piRNA interactions are highlighted in orange. Molecular entities were categorized into type (node color), degree of connection to other nodes (node size), and molecular function (node shape).

are essential contributors to immune homeostasis and participate in a diverse range of immunomodulation during the inflammatory response. These results suggest that the piRNA-mediated disruption of normal IL-6 and SOCS3 can affect the activity of different genes, which uniquely contribute to *T. cruzi* induced pathogenesis.

DISCUSSION

T. cruzi infection leads to the onset of cardiomyopathies, including cardiomegaly, cardiac fibrosis, and myocardial hypertrophy. Primary human cardiac myocytes and fibroblasts constitute good models to study how the parasite can dysregulate the expression of genes and host immune signaling pathways, potentially contributing to *T. cruzi* pathogenesis. We and others showed that the parasite dysregulates host transcription, including the miRNA expression profile through unknown mechanisms (35,41,48-51). We and others also showed that the parasite increased the expression of host transcription factors and immune molecules that facilitate infection and play roles in fibrotic responses through unknown mechanisms (6,35,52-55). Despite recent advances in our understanding of *T. cruzi* pathogenesis, the exact mechanisms through which the parasite induces fibrogenic

responses from the acute to chronic phases of infection remain poorly understood. Initially, piRNAs were thought to only maintain genomic integrity via transposon silencing in germline cells; however, more recently, piRNAs are now being implicated in the regulation of key biological processes that regulate homeostasis (56). Micro RNAs (miRNAs) and small interfering RNAs (siRNAs) have been shown to regulate transcript and protein expression via binding to target mRNAs (57,58). Analogous to miRNAs, piRNAs bind to their target genes through imperfect pairing to regulate transcription, and translation (57,58). When complexed with PIWI proteins, piRNAs play roles in transposon silencing, *de novo* methylation, chromatin remodeling, transcript stabilization, transcript degradation, and translational activation (59).

Although accumulating evidence show that piRNAs can regulate gene transcription and expression, little is known about the role of piRNAs in infectious disease research in general and specifically, during the host cell infection by *T. cruzi*. Recently, we challenged PHCM with *T. cruzi* and showed that the parasite modulates the expression profile of host piRNA during the early phase of infection (41). The roles of these dysregulated piRNAs, which were computationally predicted to target fibrotic molecules including *TGFBI*, *NFATC*, and *FOS*, among others, during *T. cruzi* infection, are under investigation in our laboratory (35,41).

Numerous reports suggest that IL-6 expression increases during early parasite infection in patients with progressive Chagas disease (60). Furthermore, IL-6 has been suggested to participate in crosstalk with TGF- β signaling to initiate fibrotic responses in various disease contexts (61-63). We and others showed that *T. cruzi* upregulates TGF- β transcript and protein to facilitate TGF- β signaling, an absolute requirement for parasite infection, multiplication, and persistence (64,65). IL-6 signaling molecules have been suggested to play essential roles in *T. cruzi* pathogenesis (6,47). Based on our previous observations in PHCM, we now report that piRNAs piR_004506, piR_001356, and piR_017716 which were not significantly dysregulated in *T. cruzi* challenged PHCM are dysregulated by the parasite in challenged PHCF (Fig. 2C, D and E). These dysregulated piRNAs were computationally predicted to target IL-6 signaling molecules using miRanda (Fig. 1A and B). These piRNAs which were first discovered in human germline cells, were yet to be implicated in *T. cruzi* pathogenesis (39). Though their differential expression in PHCM were not significant, the level of their expression in PHCF during acute *T. cruzi* infection remained unknown. Others suggested that piRNA expression is context-dependent (42,43), therefore, we challenged PHCF with *T. cruzi* for different time points and evaluated expression of these piRNAs, IL-6, and SOCS3, a downstream target of the canonical IL-6 signaling pathway that negatively regulates JAK activity and STAT3 activation (24,66).

We observed a decrease in IL-6 transcript expression during parasite challenge relative to control (Fig. 2A). The expression of piR_004506, computationally predicted to target *IL6*, showed a significant increase at 1 hour following parasite challenge relative to the control (Fig. 2C). This significant inverse relationship between target transcript expression and piRNA expression suggests that this piRNA negatively regulates *IL6* in PHCF challenged with *T. cruzi*. Accordingly, we observed a significant continuous decrease in IL-6 secretion in the condition media to a minimum at 6 h (Fig. 3B). Furthermore, sIL-6R and sgp-130 showed a significant increase at 1 h relative to control and relatively steady expression at 3 and 6 hrs in the condition media (Fig. 3). Additionally, we found no significant change in membrane bound IL-6R or gp-130 expression during the course of parasite infection (Supplementary Fig. 1). These findings differ from other reports suggesting that IL-6 expression is increased

during early parasite infection in human (41) and murine cardiac tissue (6,47) comprised of a combination of infiltrating cells, cardiac fibroblasts, and cardiomyocytes (67). However, the amount of IL-6 produced by each individual cell type contributing to the reported increase was not known, although macrophages and cardiomyocytes have been suggested to stimulate cardiac fibroblasts to produce IL-6 (28,68). Our observations of decreased IL-6 production by PHCF agrees with others suggesting that fibroblasts produce higher amounts of IL-6 in the presence of other cells. This suggests that single-cell protein and nucleotide sequencing has the potential to indicate the actual contribution of each cell type.

Next, we investigated downstream IL-6 signaling where phosphorylation of STAT3 by JAKs at the cytoplasmic tails of gp-130 activates canonical IL-6 signaling. Activated p-STAT3 is translocated to the nucleus to initiate transcription of various downstream genes, including *SOCS3* (69). We found that during parasite challenge, p-STAT3 Y705 showed steady expression and a significant increase at 6 h (Fig. 4A). In contrast, *SOCS3* exhibited significantly decreased expression during parasite challenge (Fig. 4B); these data suggest that increased p-STAT3 could be associated with decreased *SOCS3* expression. The strong inverse correlation between piR_001356, piR_017716, and *SOCS3* expression (Fig. 2B, D and E) suggests that these piRNAs function as negative regulators of *SOCS3* to sustain p-STAT3 activation. This concept is being investigated in ongoing studies in our laboratory. Overall, our data agree with others suggesting that the piRNA expression profile can be cell type and tissue dependent (43,69).

The activation of STAT3 in cardiomyocytes during *T. cruzi* infection was associated with increased expression of anti-apoptotic factors including Bcl2 to facilitate cell survival (70) facilitating *T. cruzi* infection and immune evasion (71). Other interleukin mediators such as IL-7, IL-8, IL-10, and IL-11 have also been suggested to induce STAT3-mediated effects to influence inflammatory responses were evaluated (Supplementary Fig. 2). These interleukins could mediate STAT3 activation in the absence of IL-6 through unknown mechanisms.

IL-6 signaling molecules and piRNAs were used to generate a network connecting related genes within one degree of biological interaction (Fig. 5). We observed that STAT3 participated in the most protein-protein interactions within the network. Through regulation of IL-6 and *SOCS3*, the piRNAs dysregulated by the parasite may influence the activity of several transcription factors (Zinc finger and BTB domain containing 16 [ZBTB16], melanocyte inducing transcription factor [MITF], STAT1, STAT3, and STAT5B) and tyrosine kinases (JAK1, JAK2, protein kinase C delta [PRKCD], protein tyrosine kinase 2 beta [PTK2B], and epidermal growth factor [EGF]). ZBTB16 and STAT5 have roles in regulating NK cell development and differentiation (72,73). MITF, a regulator of cell proliferation (74) has been associated with growth regulation and hypertrophy in cardiac cells through interactions with sncRNA (75). In a *T. cruzi*-infected STAT1 knockout mouse model, an imbalance of proinflammatory and anti-inflammatory cytokines was correlated with increased parasite load (52). PRKCD is established to have a role in many cardiovascular diseases including cardiac hypertrophy, arrhythmia, and cardiac fibrosis (76,77). PTK2B is required for macrophage polarization and chemotaxis (78). *T. cruzi* uses EGF-mediated signaling to regulate parasite proliferation during infection (79).

Lastly, we generated a model suggesting the operation of IL-6 signaling during early *T. cruzi* infection of PHCF (Fig. 6). IL-6 binds to sIL-6R with high affinity, this complex then binds to the membrane-bound gp-130 to activate IL-6 signaling downstream. However, soluble gp-130 can bind to the sIL-6R/IL-6 complex sequestering the complex and negatively

affecting IL-6 signaling. Once sIL-6R/IL-6 binds to mbgp-130, cytoplasmic associated JAKs become transactivated and induce phosphorylation of several tyrosine residues on the cytosolic domain of gp-130. STAT3 docks at the cytoplasmic domain of gp-130 to become phosphorylated by JAK at Y705. Activated STAT3 molecules form an active homodimer that translocate to the nucleus to induce transcription of target genes in a time-dependent manner. SOCS3, suggested to target IL-6 and negatively regulate the IL-6 signaling pathway can be potentially targeted by the piRNAs to sustain IL-6 signaling during acute *T. cruzi*

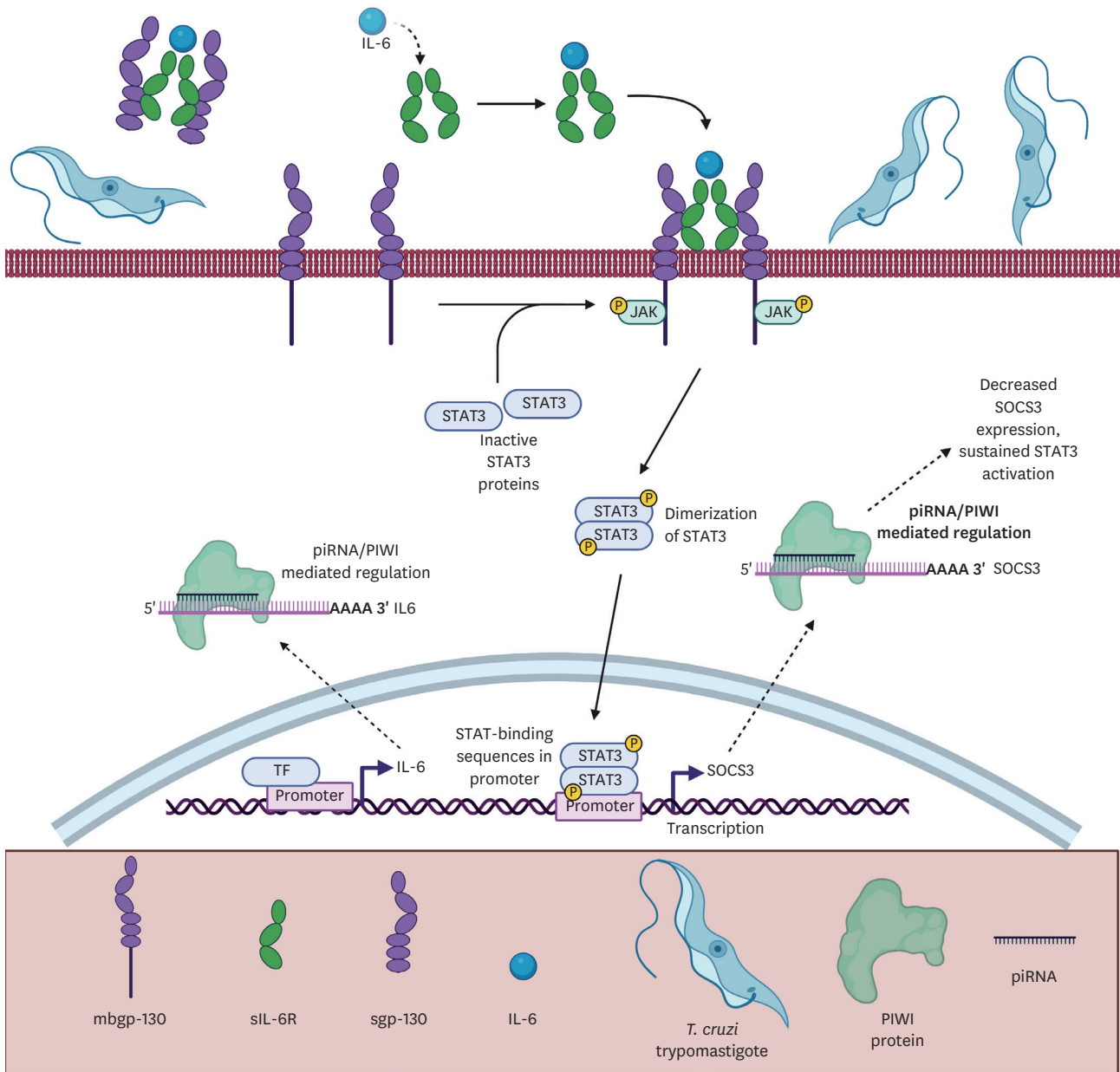


Figure 6. Model of suggested IL-6 signaling during early *T. cruzi* infection of PHCF. IL-6 binds to sIL-6R to enact receptor activation. The complex binds to mbgp-130 receptor, which becomes activated and leads to JAK phosphorylation. Activated p-JAK phosphorylates STAT3 at tyrosine Y705 to facilitate homodimerization of p-STAT3 transcription factors. The p-STAT3 homodimer is translocate to the nucleus to initiate the transcription of target genes such as SOCS3. SOCS3 traditionally inhibits IL-6 signaling. However, increased piRNA expression potentially targets and decrease SOCS3 transcript and protein expression during early infection. Accordingly, increased expression of piRNA targeting IL-6 will attenuate IL-6 transcript, protein expression and secretion during early infection of PHCF. This image was created with the assistance of BioRender.

infection. Ongoing studies in our laboratory are examining the expression of piRNAs and IL-6 signaling molecules at later time points *in vitro* and *in vivo*. To our knowledge, this constitutes the first report illustrating that *T. cruzi* induced alterations in the expression of piRNAs computationally predicted to target the IL-6 signaling in PHCF.

Our results suggest that the fibroblast response to *T. cruzi* challenge may be different from other cardiac cell types, which was one of our expectations. Additionally, the dysregulated piRNAs potentially function as negative regulators of IL-6 and SOCS3 to adjust the inflammatory response during early infection. The observed decrease in IL-6 secretion and mRNA expression accompanied by decreased SOCS3 protein and mRNA expression suggests that a robust SOCS3 mediated regulation may not be essential, allowing for a sustained p-STAT3 activation. More studies are needed to determine if this dysregulation is parasite induced or host response to decrease inflammation and reduce infection. Additionally, further studies are needed to elucidate their full function during *T. cruzi* pathogenesis. A detailed understanding of the role of piRNAs as potential key regulators of biological processes including signaling and gene expression in *T. cruzi* infected primary cells during acute and chronic infections can lead to the identification of new biomarkers and molecular intervention strategies.

ACKNOWLEDGEMENTS

We are grateful to the Molecular Biology Core Facility and the Morphology Core at Meharry Medical College. This work was supported by NIH grants 1SC1AI27352 (PNN), 2T32AI007281-31 (AC), 2T32HL007737-26 (AC), 5R25GM05994 (KJR), F31AI167579 (KJR), and U54MD007586 (FV). The funders had no role in the study design, data collection, and analysis, decision to publish, or preparation of the manuscript.

SUPPLEMENTARY MATERIALS

Supplemental Figure 1

Flow cytometry evaluation of cell surface IL-6R and gp130 expression. Parasite challenged PHCF were trypsinized and stained with anti-CD126 (IL-6R) and anti-CD130 (gp-130) Abs for 30 min at 4 °C. Cells were analyzed for surface protein expression using Amnis CellStream Flow Cytometer. Single cells were gated for live cells and evaluated for surface protein staining at (A) 0 h, (B) 1 h, (C) 3 h, and (D) 6 h. Visualization and statistical analysis of (E) CD130 (gp-130) and (F) CD126 (IL-6R) expression was completed using Student's *t*-test in GraphPad. Mean values of biological replicates \pm SEM.

[Click here to view](#)

Supplementary Figure 2

Cytokine array analysis of IL-7, IL-8, IL-10, and IL-11 in condition media of *T. cruzi*-challenged primary human cardiac fibroblasts. Condition media of PHCF challenged with *T. cruzi* at multiple time points were incubated with cytokine array membranes. Spots were quantified using ImageJ and normalized to positive control spots. Bar graph depicting fold change of (A) IL-7 (B) IL-8, (C) IL-10, and (D) IL-11 mean spot densities relative to positive controls in condition media of PHCF *T. cruzi* challenged cells. Mean values of biological replicates \pm

SEM are shown. Visualization was created and statistical significance was calculated using Student's *t*-test in GraphPad Prism.

[Click here to view](#)

REFERENCES

1. Abuhab A, Trindade E, Aulicino GB, Fujii S, Bocchi EA, Bacal F. Chagas' cardiomyopathy: the economic burden of an expensive and neglected disease. *Int J Cardiol* 2013;168:2375-2380.
[PUBMED](#) | [CROSSREF](#)
2. Olivera MJ, Buitrago G. Economic costs of Chagas disease in Colombia in 2017: a social perspective. *Int J Infect Dis* 2020;91:196-201.
[PUBMED](#) | [CROSSREF](#)
3. Lidani KC, Andrade FA, Bavia L, Damasceno FS, Beltrame MH, Messias-Reason IJ, Sandri TL. Chagas disease: from discovery to a worldwide health problem. *Front Public Health* 2019;7:166.
[PUBMED](#) | [CROSSREF](#)
4. Nunes MCP, Beaton A, Acquatella H, Bern C, Bolger AF, Echeverría LE, Dutra WO, Gascon J, Morillo CA, Oliveira-Filho J, et al. Chagas cardiomyopathy: an update of current clinical knowledge and management: a scientific statement from the American Heart Association. *Circulation* 2018;138:e169-e209.
[PUBMED](#) | [CROSSREF](#)
5. Gomes Dos Santos A, Watanabe EH, Ferreira DT, Oliveira J, Nakanishi ES, Oliveira CS, Bocchi E, Novaes CTG, Cruz F, Carvalho NB, et al. A specific *IL6* polymorphic genotype modulates the risk of *Trypanosoma cruzi* parasitemia while *IL18*, *IL17A*, and *IL1B* variant profiles and HIV infection protect against cardiomyopathy in Chagas disease. *Front Immunol* 2020;11:521409.
[PUBMED](#) | [CROSSREF](#)
6. Hoffman KA, Villar MJ, Poveda C, Bottazzi ME, Hotez PJ, Twardy DJ, Jones KM. Signal transducer and activator of transcription-3 modulation of cardiac pathology in chronic Chagasic cardiomyopathy. *Front Cell Infect Microbiol* 2021;11:708325.
[PUBMED](#) | [CROSSREF](#)
7. López L, Arai K, Giménez E, Jiménez M, Pascuzo C, Rodríguez-Bonfante C, Bonfante-Cabarcas R. C-reactive protein and interleukin-6 serum levels increase as Chagas disease progresses towards cardiac failure. *Rev Esp Cardiol* 2006;59:50-56.
[PUBMED](#)
8. Fielding CA, Jones GW, McLoughlin RM, McLeod L, Hammond VJ, Uceda J, Williams AS, Lambie M, Foster TL, Liao CT, et al. Interleukin-6 signaling drives fibrosis in unresolved inflammation. *Immunity* 2014;40:40-50.
[PUBMED](#) | [CROSSREF](#)
9. Gabay C. Interleukin-6 and chronic inflammation. *Arthritis Res Ther* 2006;8 Suppl 2:S3.
[PUBMED](#) | [CROSSREF](#)
10. Hirano T. IL-6 in inflammation, autoimmunity and cancer. *Int Immunol* 2021;33:127-148.
[PUBMED](#) | [CROSSREF](#)
11. Kishimoto T. IL-6: from its discovery to clinical applications. *Int Immunol* 2010;22:347-352.
[PUBMED](#) | [CROSSREF](#)
12. Chi L, Li Y, Stehno-Bittel L, Gao J, Morrison DC, Stechschulte DJ, Dileepan KN. Interleukin-6 production by endothelial cells via stimulation of protease-activated receptors is amplified by endotoxin and tumor necrosis factor-alpha. *J Interferon Cytokine Res* 2001;21:231-240.
[PUBMED](#) | [CROSSREF](#)
13. Nguyen HN, Noss EH, Mizoguchi F, Huppertz C, Wei KS, Watts GF, Brenner MB. Autocrine loop involving IL-6 family member LIF, LIF receptor, and STAT4 drives sustained fibroblast production of inflammatory mediators. *Immunity* 2017;46:220-232.
[PUBMED](#) | [CROSSREF](#)
14. Gubernatorova EO, Gorshkova EA, Polinova AI, Drutskaya MS. IL-6: relevance for immunopathology of SARS-CoV-2. *Cytokine Growth Factor Rev* 2020;53:13-24.
[PUBMED](#) | [CROSSREF](#)
15. Galun E, Rose-John S. The regenerative activity of interleukin-6. *Methods Mol Biol* 2013;982:59-77.
[PUBMED](#) | [CROSSREF](#)

16. Johnson BZ, Stevenson AW, Prêle CM, Fear MW, Wood FM. The role of IL-6 in skin fibrosis and cutaneous wound healing. *Biomedicines* 2020;8:101.
[PUBMED](#) | [CROSSREF](#)
17. Yue B. Biology of the extracellular matrix: an overview. *J Glaucoma* 2014;23:S20-S23.
[PUBMED](#) | [CROSSREF](#)
18. Peng CY, Liao YW, Lu MY, Yang CM, Hsieh PL, Yu CC. Positive feedback loop of Snail-IL-6 mediates myofibroblastic differentiation activity in precancerous oral submucous fibrosis. *Cancers (Basel)* 2020;12:E1611.
[PUBMED](#) | [CROSSREF](#)
19. Hinz B. The role of myofibroblasts in wound healing. *Curr Res Transl Med* 2016;64:171-177.
[PUBMED](#) | [CROSSREF](#)
20. Klingberg F, Hinz B, White ES. The myofibroblast matrix: implications for tissue repair and fibrosis. *J Pathol* 2013;229:298-309.
[PUBMED](#) | [CROSSREF](#)
21. Schumacher N, Meyer D, Mauermann A, von der Heyde J, Wolf J, Schwarz J, Knittler K, Murphy G, Michalek M, Garbers C, et al. Shedding of endogenous interleukin-6 receptor (IL-6R) is governed by a disintegrin and metalloproteinase (ADAM) proteases while a full-length IL-6R isoform localizes to circulating microvesicles. *J Biol Chem* 2015;290:26059-26071.
[PUBMED](#) | [CROSSREF](#)
22. Jones SA, Rose-John S. The role of soluble receptors in cytokine biology: the agonistic properties of the sIL-6R/IL-6 complex. *Biochim Biophys Acta* 2002;1592:251-263.
[PUBMED](#) | [CROSSREF](#)
23. Müllberg J, Schooltink H, Stoyan T, Günther M, Graeve L, Buse G, Mackiewicz A, Heinrich PC, Rose-John S. The soluble interleukin-6 receptor is generated by shedding. *Eur J Immunol* 1993;23:473-480.
[PUBMED](#) | [CROSSREF](#)
24. Niemand C, Nimmesgern A, Haan S, Fischer P, Schaper F, Rossaint R, Heinrich PC, Müller-Newen G. Activation of STAT3 by IL-6 and IL-10 in primary human macrophages is differentially modulated by suppressor of cytokine signaling 3. *J Immunol* 2003;170:3263-3272.
[PUBMED](#) | [CROSSREF](#)
25. O'Reilly S, Ciecchomska M, Cant R, van Laar JM. Interleukin-6 (IL-6) trans signaling drives a STAT3-dependent pathway that leads to hyperactive transforming growth factor- β (TGF- β) signaling promoting SMAD3 activation and fibrosis via Gremlin protein. *J Biol Chem* 2014;289:9952-9960.
[PUBMED](#) | [CROSSREF](#)
26. Reeh H, Rudolph N, Billing U, Christen H, Streif S, Bullinger E, Schliemann-Bullinger M, Findeisen R, Schaper F, Huber HJ, et al. Response to IL-6 trans- and IL-6 classic signalling is determined by the ratio of the IL-6 receptor α to gp130 expression: fusing experimental insights and dynamic modelling. *Cell Commun Signal* 2019;17:46.
[PUBMED](#) | [CROSSREF](#)
27. Murakami M, Kamimura D, Hirano T. Pleiotropy and specificity: insights from the interleukin 6 family of cytokines. *Immunity* 2019;50:812-831.
[PUBMED](#) | [CROSSREF](#)
28. Fredj S, Bescond J, Louault C, Delwail A, Lecron JC, Potreau D. Role of interleukin-6 in cardiomyocyte/cardiac fibroblast interactions during myocyte hypertrophy and fibroblast proliferation. *J Cell Physiol* 2005;204:428-436.
[PUBMED](#) | [CROSSREF](#)
29. Kumar S, Wang G, Zheng N, Cheng W, Ouyang K, Lin H, Liao Y, Liu J. HIMF (hypoxia-induced mitogenic factor)-IL (interleukin)-6 signaling mediates cardiomyocyte-fibroblast crosstalk to promote cardiac hypertrophy and fibrosis. *Hypertension* 2019;73:1058-1070.
[PUBMED](#) | [CROSSREF](#)
30. Lai YH, Lo CI, Wu YJ, Hung CL, Yeh HI. Cardiac remodeling, adaptations and associated myocardial mechanics in hypertensive heart diseases. *Zhonghua Minguo Xinzangxue Hui Zazhi* 2013.29:64-70.
[PUBMED](#)
31. Yajima T, Murofushi Y, Zhou H, Park S, Housman J, Zhong ZH, Nakamura M, Machida M, Hwang KK, Gu Y, et al. Absence of SOCS3 in the cardiomyocyte increases mortality in a gp130-dependent manner accompanied by contractile dysfunction and ventricular arrhythmias. *Circulation* 2011;124:2690-2701.
[PUBMED](#) | [CROSSREF](#)
32. Rodríguez-Angulo H, Marques J, Mendoza I, Villegas M, Mijares A, Gironès N, Fresno M. Differential cytokine profiling in Chagasic patients according to their arrhythmogenic-status. *BMC Infect Dis* 2017;17:221.
[PUBMED](#) | [CROSSREF](#)

33. Rodríguez-Angulo HO, Colombet-Naranjo D, Maza MC, Poveda C, Herreros-Cabello A, Mendoza I, Perera JC, Goyo JD, Gironès N, Fresno M. Molecular remodeling of cardiac sinus node associated with acute Chagas disease myocarditis. *Microorganisms* 2021;9:2208.
[PUBMED](#) | [CROSSREF](#)
34. Antunes D, Marins-Dos-Santos A, Ramos MT, Mascarenhas BA, Moreira CJ, Farias-de-Oliveira DA, Savino W, Monteiro RQ, de Meis J. Oral route driven acute *Trypanosoma cruzi* infection unravels an IL-6 dependent hemostatic derangement. *Front Immunol* 2019;10:1073.
[PUBMED](#) | [CROSSREF](#)
35. Udoko AN, Johnson CA, Dykan A, Rachakonda G, Villalta F, Mandape SN, Lima MF, Pratap S, Nde PN. Early regulation of profibrotic genes in primary human cardiac myocytes by *Trypanosoma cruzi*. *PLoS Negl Trop Dis* 2016;10:e0003747.
[PUBMED](#) | [CROSSREF](#)
36. Volta BJ, Bustos PL, Cardoni RL, De Rissio AM, Laucella SA, Bua J. Serum cytokines as biomarkers of early *Trypanosoma cruzi* infection by congenital exposure. *J Immunol* 2016;196:4596-4602.
[PUBMED](#) | [CROSSREF](#)
37. Rayford KJ, Cooley A, Rumph JT, Arun A, Rachakonda G, Villalta F, Lima MF, Pratap S, Misra S, Nde PN. piRNAs as modulators of disease pathogenesis. *Int J Mol Sci* 2021;22:2373.
[PUBMED](#) | [CROSSREF](#)
38. Simonelig M. piRNAs, master regulators of gene expression. *Cell Res* 2014;24:779-780.
[PUBMED](#) | [CROSSREF](#)
39. Girard A, Sachidanandam R, Hannon GJ, Carmell MA. A germline-specific class of small RNAs binds mammalian PIWI proteins. *Nature* 2006;442:199-202.
[PUBMED](#) | [CROSSREF](#)
40. Zhong F, Zhou N, Wu K, Guo Y, Tan W, Zhang H, Zhang X, Geng G, Pan T, Luo H, et al. A SnoRNA-derived piRNA interacts with human interleukin-4 pre-mRNA and induces its decay in nuclear exosomes. *Nucleic Acids Res* 2015;43:10474-10491.
[PUBMED](#) | [CROSSREF](#)
41. Rayford KJ, Cooley A, Arun A, Rachakonda G, Kleschenko Y, Villalta F, Pratap S, Lima MF, Nde PN. *Trypanosoma cruzi* modulates PIWI-interacting RNA expression in primary human cardiac myocytes during the early phase of infection. *Int J Mol Sci* 2020;21:E9439.
[PUBMED](#) | [CROSSREF](#)
42. Gebert D, Neubert LK, Lloyd C, Gui J, Lehmann R, Teixeira FK. Large *Drosophila* germline piRNA clusters are evolutionarily labile and dispensable for transposon regulation. *Mol Cell* 2021;81:3965-3978.e5.
[PUBMED](#) | [CROSSREF](#)
43. Martinez VD, Vucic EA, Thu KL, Hubaux R, Enfield KS, Pikor LA, Becker-Santos DD, Brown CJ, Lam S, Lam WL. Unique somatic and malignant expression patterns implicate PIWI-interacting RNAs in cancer-type specific biology. *Sci Rep* 2015;5:10423.
[PUBMED](#) | [CROSSREF](#)
44. Arun A, Rayford KJ, Cooley A, Rana T, Rachakonda G, Villalta F, Pratap S, Lima MF, Sheibani N, Nde PN. Thrombospondin-1 expression and modulation of Wnt and hippo signaling pathways during the early phase of *Trypanosoma cruzi* infection of heart endothelial cells. *PLoS Negl Trop Dis* 2022;16:e0010074.
[PUBMED](#) | [CROSSREF](#)
45. Schneider CA, Rasband WS, Eliceiri KW. NIH image to ImageJ: 25 years of image analysis. *Nat Methods* 2012;9:671-675.
[PUBMED](#) | [CROSSREF](#)
46. Warde-Farley D, Donaldson SL, Comes O, Zuberi K, Badrawi R, Chao P, Franz M, Grouios C, Kazi F, Lopes CT, et al. The GeneMANIA prediction server: biological network integration for gene prioritization and predicting gene function. *Nucleic Acids Res* 2010;38:W214-W220.
[PUBMED](#) | [CROSSREF](#)
47. Ponce NE, Carrera-Silva EA, Pellegrini AV, Cazorla SI, Malchiodi EL, Lima AP, Gea S, Aoki MP. *Trypanosoma cruzi*, the causative agent of Chagas disease, modulates interleukin-6-induced STAT3 phosphorylation via gp130 cleavage in different host cells. *Biochim Biophys Acta* 2013;1832:485-494.
[PUBMED](#) | [CROSSREF](#)
48. Ferreira LR, Ferreira FM, Laugier L, Cabantous S, Navarro IC, da Silva Cândido D, Rigaud VC, Real JM, Pereira GV, Pereira IR, et al. Integration of miRNA and gene expression profiles suggest a role for miRNAs in the pathobiological processes of acute *Trypanosoma cruzi* infection. *Sci Rep* 2017;7:17990.
[PUBMED](#) | [CROSSREF](#)
49. Laugier L, Ferreira LR, Ferreira FM, Cabantous S, Frade AF, Nunes JP, Ribeiro RA, Brochet P, Teixeira PC, Santos RH, et al. miRNAs may play a major role in the control of gene expression in key pathobiological processes in Chagas disease cardiomyopathy. *PLoS Negl Trop Dis* 2020;14:e0008889.
[PUBMED](#) | [CROSSREF](#)

50. Nisimura LM, Coelho LL, de Melo TG, Vieira PC, Victorino PH, Garzoni LR, Spray DC, Iacobas DA, Iacobas S, Tanowitz HB, et al. *Trypanosoma cruzi* promotes transcriptomic remodeling of the JAK/STAT signaling and cell cycle pathways in myoblasts. *Front Cell Infect Microbiol* 2020;10:255.
[PUBMED](#) | [CROSSREF](#)
51. Oliveira AER, Pereira MCA, Belew AT, Ferreira LRP, Pereira LMN, Neves EGA, Nunes MDCP, Burleigh BA, Dutra WO, El-Sayed NM, et al. Gene expression network analyses during infection with virulent and avirulent *Trypanosoma cruzi* strains unveil a role for fibroblasts in neutrophil recruitment and activation. *PLoS Pathog* 2020;16:e1008781.
[PUBMED](#) | [CROSSREF](#)
52. Kulkarni MM, Varikuti S, Terrazas C, Kimble JL, Satoskar AR, McGwire BS. Signal transducer and activator of transcription 1 (STAT-1) plays a critical role in control of *Trypanosoma cruzi* infection. *Immunology* 2015;145:225-231.
[PUBMED](#) | [CROSSREF](#)
53. Navarro IC, Ferreira FM, Nakaya HI, Baron MA, Vilar-Pereira G, Pereira IR, Silva AM, Real JM, De Brito T, Chevillard C, et al. MicroRNA transcriptome profiling in heart of *Trypanosoma cruzi*-infected mice: parasitological and cardiological outcomes. *PLoS Negl Trop Dis* 2015;9:e0003828.
[PUBMED](#) | [CROSSREF](#)
54. Suman S, Rachakonda G, Mandape SN, Sakhare SS, Villalta F, Pratap S, Lima MF, Nde PN. Phospho-proteomic analysis of primary human colon epithelial cells during the early *Trypanosoma cruzi* infection phase. *PLoS Negl Trop Dis* 2018;12:e0006792.
[PUBMED](#) | [CROSSREF](#)
55. Thiruvankatarajan V, Meyer EJ, Jesudason D. Comment on Hamblin et al. Capillary ketone concentrations at the time of colonoscopy: a cross-sectional study with implications for SGLT2 inhibitor-treated type 2 diabetes. *Diabetes Care* 2021;44:e124-e126. *Diabetes Care* 2022;45:e15-e16.
[PUBMED](#) | [CROSSREF](#)
56. Jones BC, Wood JG, Chang C, Tam AD, Franklin MJ, Siegel ER, Helfand SL. A somatic piRNA pathway in the *Drosophila* fat body ensures metabolic homeostasis and normal lifespan. *Nat Commun* 2016;7:13856.
[PUBMED](#) | [CROSSREF](#)
57. Huang S, Yoshitake K, Asakawa S. A review of discovery profiling of PIWI-interacting RNAs and their diverse functions in metazoans. *Int J Mol Sci* 2021;22:11166.
[PUBMED](#) | [CROSSREF](#)
58. Weick EM, Miska EA. piRNAs: from biogenesis to function. *Development* 2014;141:3458-3471.
[PUBMED](#) | [CROSSREF](#)
59. Watanabe T, Lin H. Posttranscriptional regulation of gene expression by Piwi proteins and piRNAs. *Mol Cell* 2014;56:18-27.
[PUBMED](#) | [CROSSREF](#)
60. Herrera RN, Díaz de Amaya EI, Pérez Aguilar RC, Joo Turoni C, Marañón R, Berman SG, Luciardi HL, Coviello A, Peral de Bruno M. Inflammatory and prothrombotic activation with conserved endothelial function in patients with chronic, asymptomatic Chagas disease. *Clin Appl Thromb Hemost* 2011;17:502-507.
[PUBMED](#) | [CROSSREF](#)
61. McGeachy MJ, Bak-Jensen KS, Chen Y, Tato CM, Blumenschein W, McClanahan T, Cua DJ. TGF-beta and IL-6 drive the production of IL-17 and IL-10 by T cells and restrain T(H)-17 cell-mediated pathology. *Nat Immunol* 2007;8:1390-1397.
[PUBMED](#) | [CROSSREF](#)
62. Yamada D, Kobayashi S, Wada H, Kawamoto K, Marubashi S, Eguchi H, Ishii H, Nagano H, Doki Y, Mori M. Role of crosstalk between interleukin-6 and transforming growth factor-beta 1 in epithelial-mesenchymal transition and chemoresistance in biliary tract cancer. *Eur J Cancer* 2013;49:1725-1740.
[PUBMED](#) | [CROSSREF](#)
63. Zhang XL, Topley N, Ito T, Phillips A. Interleukin-6 regulation of transforming growth factor (TGF)-beta receptor compartmentalization and turnover enhances TGF-beta1 signaling. *J Biol Chem* 2005;280:12239-12245.
[PUBMED](#) | [CROSSREF](#)
64. Waghbi MC, Keramidas M, Calvet CM, Meuser M, de Nazaré C Soeiro M, Mendonça-Lima L, Araújo-Jorge TC, Feige JJ, Bailly S. SB-431542, a transforming growth factor beta inhibitor, impairs *Trypanosoma cruzi* infection in cardiomyocytes and parasite cycle completion. *Antimicrob Agents Chemother* 2007;51:2905-2910.
[PUBMED](#) | [CROSSREF](#)
65. Waghbi MC, Keramidas M, Feige JJ, Araújo-Jorge TC, Bailly S. Activation of transforming growth factor beta by *Trypanosoma cruzi*. *Cell Microbiol* 2005;7:511-517.
[PUBMED](#) | [CROSSREF](#)

66. Zhu BM, Ishida Y, Robinson GW, Pacher-Zavisin M, Yoshimura A, Murphy PM, Hennighausen L. SOCS3 negatively regulates the gp130-STAT3 pathway in mouse skin wound healing. *J Invest Dermatol* 2008;128:1821-1829.
[PUBMED](#) | [CROSSREF](#)
67. Truyens C, Angelo-Barrios A, Torrico F, Van Damme J, Heremans H, Carlier Y. Interleukin-6 (IL-6) production in mice infected with *Trypanosoma cruzi*: effect of its paradoxical increase by anti-IL-6 monoclonal antibody treatment on infection and acute-phase and humoral immune responses. *Infect Immun* 1994;62:692-696.
[PUBMED](#) | [CROSSREF](#)
68. Ma F, Li Y, Jia L, Han Y, Cheng J, Li H, Qi Y, Du J. Macrophage-stimulated cardiac fibroblast production of IL-6 is essential for TGF β /Smad activation and cardiac fibrosis induced by angiotensin II. *PLoS One* 2012;7:e35144.
[PUBMED](#) | [CROSSREF](#)
69. Cevey AC, Penas FN, Alba Soto CD, Mirkin GA, Goren NB. IL-10/STAT3/SOCS3 axis is involved in the anti-inflammatory effect of benznidazole. *Front Immunol* 2019;10:1267.
[PUBMED](#) | [CROSSREF](#)
70. Stahl P, Schwarz RT, Debierre-Grockiego F, Meyer T. *Trypanosoma cruzi* parasites fight for control of the JAK-STAT pathway by disarming their host. *JAK-STAT* 2015;3:e1012964.
[PUBMED](#) | [CROSSREF](#)
71. Ponce NE, Cano RC, Carrera-Silva EA, Lima AP, Gea S, Aoki MP. Toll-like receptor-2 and interleukin-6 mediate cardiomyocyte protection from apoptosis during *Trypanosoma cruzi* murine infection. *Med Microbiol Immunol (Berl)* 2012;201:145-155.
[PUBMED](#) | [CROSSREF](#)
72. Cheng ZY, He TT, Gao XM, Zhao Y, Wang J. ZBTB transcription factors: key regulators of the development, differentiation and effector function of T cells. *Front Immunol* 2021;12:713294.
[PUBMED](#) | [CROSSREF](#)
73. Gotthardt D, Trifinopoulos J, Sexl V, Putz EM. JAK/STAT cytokine signaling at the crossroad of NK cell development and maturation. *Front Immunol* 2019;10:2590.
[PUBMED](#) | [CROSSREF](#)
74. Hershey CL, Fisher DE. Genomic analysis of the *Microphthalmia* locus and identification of the MITF-*J* Mitf-*J* isoform. *Gene* 2005;347:73-82.
[PUBMED](#) | [CROSSREF](#)
75. Tshori S, Gilon D, Beeri R, Nechushtan H, Kaluzhny D, Pikarsky E, Razin E. Transcription factor MITF regulates cardiac growth and hypertrophy. *J Clin Invest* 2006;116:2673-2681.
[PUBMED](#) | [CROSSREF](#)
76. Braun MU, Mochly-Rosen D. Opposing effects of delta- and zeta-protein kinase C isozymes on cardiac fibroblast proliferation: use of isozyme-selective inhibitors. *J Mol Cell Cardiol* 2003;35:895-903.
[PUBMED](#) | [CROSSREF](#)
77. Ferreira JC, Mochly-Rosen D, Boutjdir M. Regulation of cardiac excitability by protein kinase C isozymes. *Front Biosci (Schol Ed)* 2012;4:532-546.
[PUBMED](#) | [CROSSREF](#)
78. Hinterseher I, Schworer CM, Lillvis JH, Stahl E, Erdman R, Gatalica Z, Tromp G, Kuivaniemi H. Immunohistochemical analysis of the natural killer cell cytotoxicity pathway in human abdominal aortic aneurysms. *Int J Mol Sci* 2015;16:11196-11212.
[PUBMED](#) | [CROSSREF](#)
79. Ghansah TJ, Ager EC, Freeman-Junior P, Villalta F, Lima MF. Epidermal growth factor binds to a receptor on *Trypanosoma cruzi* amastigotes inducing signal transduction events and cell proliferation. *J Eukaryot Microbiol* 2002;49:383-390.
[PUBMED](#) | [CROSSREF](#)